Transactions on Energy Systems and Engineering Applications

Article

Design of PV fed single-switch transformer less topology powered electric vehicle

Jeetender Vemula [1,2,*], E. Vidya Sagar [1], Tellapati Anuradha Devi [3], Gundala Srinivasa Rao [4], Rekha Rangam [5] and S. Venkata Rami Reddy[6]

[1] Department Electrical and Electronics Engineering, Osmania University, Hyderabad, Telangana, India.
[2] Department of Electrical and Electronics Engineering, Vignana Bharathi institute of technology, Hyderabad, India
[3] Department Electrical and Electronics Engineering, Vardhaman College of Engineering, Shamshabad, Hyderabad, India.
[4] Department of Electrical and Electronics Engineering, CMR College of Engineering & Technology, Hyderabad, India.
[5] Department of Electrical and Electronics Engineering, Anurag University, Hyderabad, India
[6] Department of Electrical and Electronics Engineering, JNTUA College of Engineering Pulivendula, Pulivendula, India.
[*] Correspondence: jeetender.eee@gmail.com

Received: 15 October 2023; Accepted: 08 June 2024; Published: 31 July 2024

Abstract: As a result of an increase in the availability of resources that were not harmful to the environment, solar energy applications shot to popularity. Photovoltaic cells power systems that necessitate DC-DC converters because of their low voltage output. This investigation uses photovoltaic cells (PV) to power a high-voltage gain design with just one switch and no transformer. The proposed circuit utilizes a single regulated switch, which contributes to a reduction in switching losses. It requires fundamental pulse regulation. The network used a switched capacitor cell and an LC passive filter to provide an accurate step-up voltage. We can obtain the equation for the step-up voltage gain from the steady-state continuous conduction mode. The equations used for the theoretical design of converters include energy. To show that the topology is comparable with other modern converters that have been published, a comparison was made between it and other converters. In order to validate the converter's effectiveness, simulations built in MATLAB and Simulink are used.

1. Introduction

Cars running on gasoline release more pollutants. Electric vehicles achieve the best emission reduction. For reasons of both the environment and the economy, electric cars perform better than petrol cars for both environmental and economic reasons. Developments in motor and battery technology will replace gasoline cars. For electric vehicles, brushless DC motors offer the best power densities, efficiency, speed-torque characteristics, wide speed ranges, and low maintenance. The circuitry of complexity controls them.

How to cite this article: Jeetender Vemula; E. Vidya Sagar; T. Anuradha Devi; Srinivasa Rao Gundala; Rekha Rangam;S. Venkata Rami Reddy . Design of PV fed single-switch transformer less topology powered electric vehicle. *Transactions on Energy Systems and Engineering Applications*, 5(2): 571, 2024. DOI:10.32397/tesea.vol5.n2.571

Batteries in electric cars are lithium and nickel. Since batteries last, applications for electric vehicles prioritize range and endurance. Batteries and motor management determine the efficiency of electric vehicles. Chemical batteries store energy for industry. Lead acid gel cells are low-maintenance. Electric automobiles have to get the most out of their batteries. Brake resistance heats conventional brake control circuits. Regenerative brakes in gasoline cars can recover energy. This leads to a decrease in pollution, improves economy, and reduces fuel consumption. Boost converters have a lower voltage boost and higher switching stress [1,2]. Largely boosted DC-DC converters are necessary to connect low-voltage DC sources to either high-voltage loads or the public power grid. Over the past decade, manufacturers have produced both isolated and non-isolated high-step-up DC-DC converters. In low and medium voltage applications, isolated converters suffer transformer core saturation, extra components, and worse efficiency [3, 4]. The voltage stress of the isolated converter is equivalent to the output voltage, even when the switch is boosting. One uses an intermediary capacitor to raise the voltage between the source and the load [5]. Charges and discharges of the capacitors occur in parallel [6–8]. The literature describes a practical voltage-boosting approach for L-C links [9]. Converters use mono switches to boost DC-voltage gain [5–9]. Parallel-connected inductor networks also produce higher gains [10]. Each network has two switches. The third switch addition increases voltage gain [11]. The converter can only increase voltage between 0.8 and d. Therefore, it is difficult to get such a great advantage. A gain cell and voltage booster system cascaded together produce a gain of $(2 - d)$ [12]. Adding an active L-C network to the existing network boosts the extra gain from $2d$ to $2/(1 - d)$ [13–16]. Gain increases with cascading capacitors [13]. In a previous study [14], the source current is intermittent. In another work [15], there are two converter switches listed. The addition of a capacitor-diode circuit from [10] boosts the voltage to $(3 - d)/(1 - d)$ [17].

Several converters using buck-boost and quadratic boost technology increase gain [18–21]. When $d < 0.7$, there is a higher voltage gain. By changing the converter [10], one can raise the voltage to $(1 + d - d2)/(1 - d)2$ [22]. Put between the load and the active inductor network [23] contains a circuit that may double the voltage. The literature [24–27] describes extensional high-gain DC-DC converters. Several works [24–27] describe converters with switches. The voltage gain does not rise appreciably when the quantity of individual components increases in long stages [25, 26]. As its name suggests, a brushless DC motor electronically commutes its brushes. More energy-efficient products come onto the market as the economy and production rise, more energy-efficient products become available. People, as well as businesses, use these products. An environmentally benign electrical industry development are brushless DC motors with rare-earth permanent magnets. These motors are small, lightweight, precise, have minimal rotational inertia, and are highly efficient. Its rotational inertia is likewise quite low. Its robust mechanical characteristics, akin to those of standard DC motors, make it suitable for variable-speed drive applications such as electric vehicle (EV) drive systems.

2. Operation of the proposed converter (SSIN)

Fig. 1(a) displays the n-stage SSIN converter. Each step, save the first, needs an inductor and three diodes. Fig. 1(b) illustrates the single-stage SSIN converter circuit for n = 1. The single-stage SSIN converter also contains a semiconductor switch, three capacitors, two inductors, six diodes, and two inductors. Switch S charges the input source's inductors L1 and L2, which discharge energy to the cross-connected capacitors C1 and C2. Linked capacitors have a double converter voltage. CCM converters. Switches control the CCM and DCM SSIN converter modes. Fig. 1(c & d) shows CCM and DCM SSIN converter analytical waveforms.

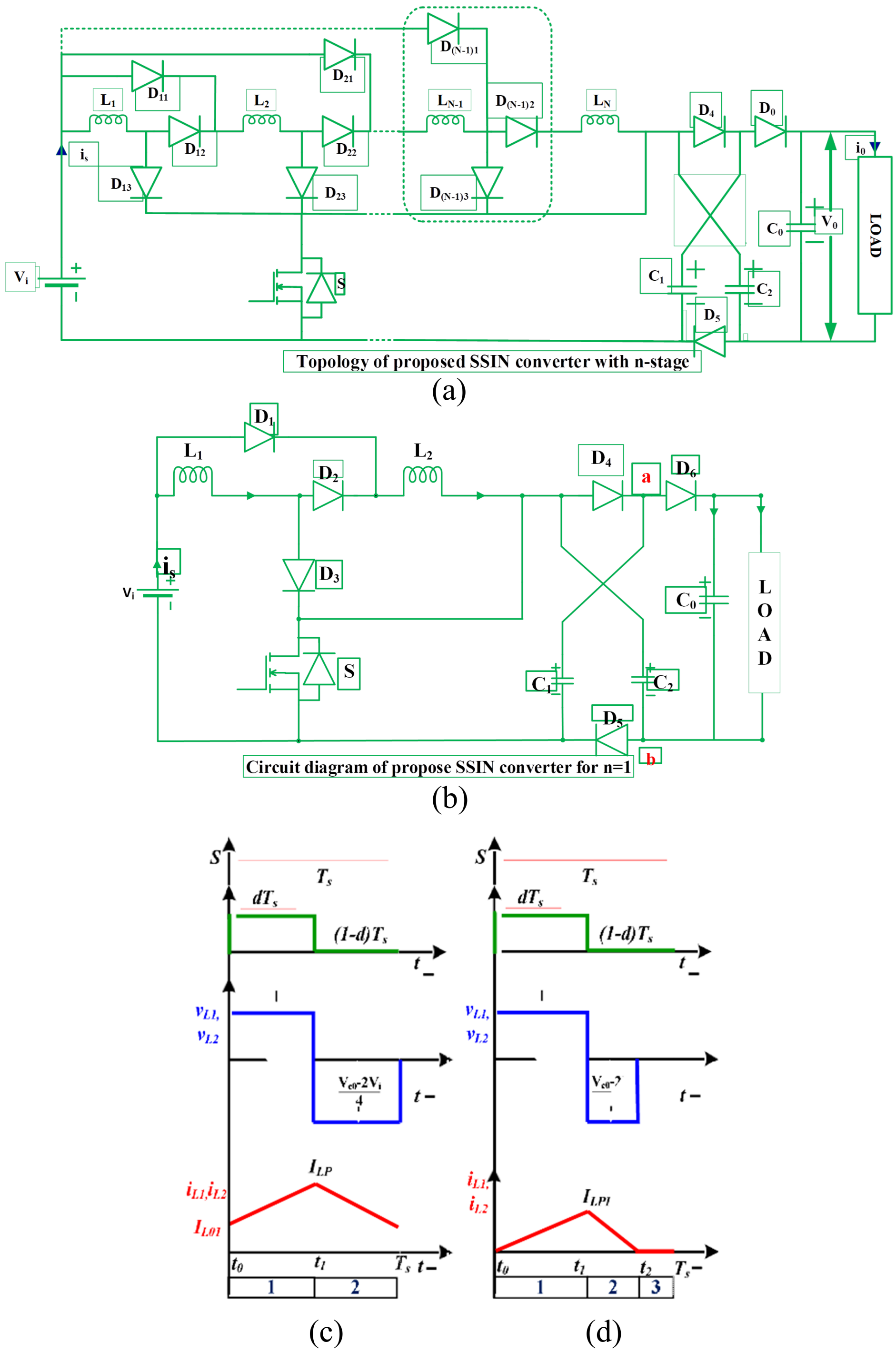

Figure 1. (a) Proposed n-stage SSIN converter topology. (b) Proposed SSIN converter circuit for n = 1. (c & d) Analytical SSIN converter CCM and DCM waveforms.

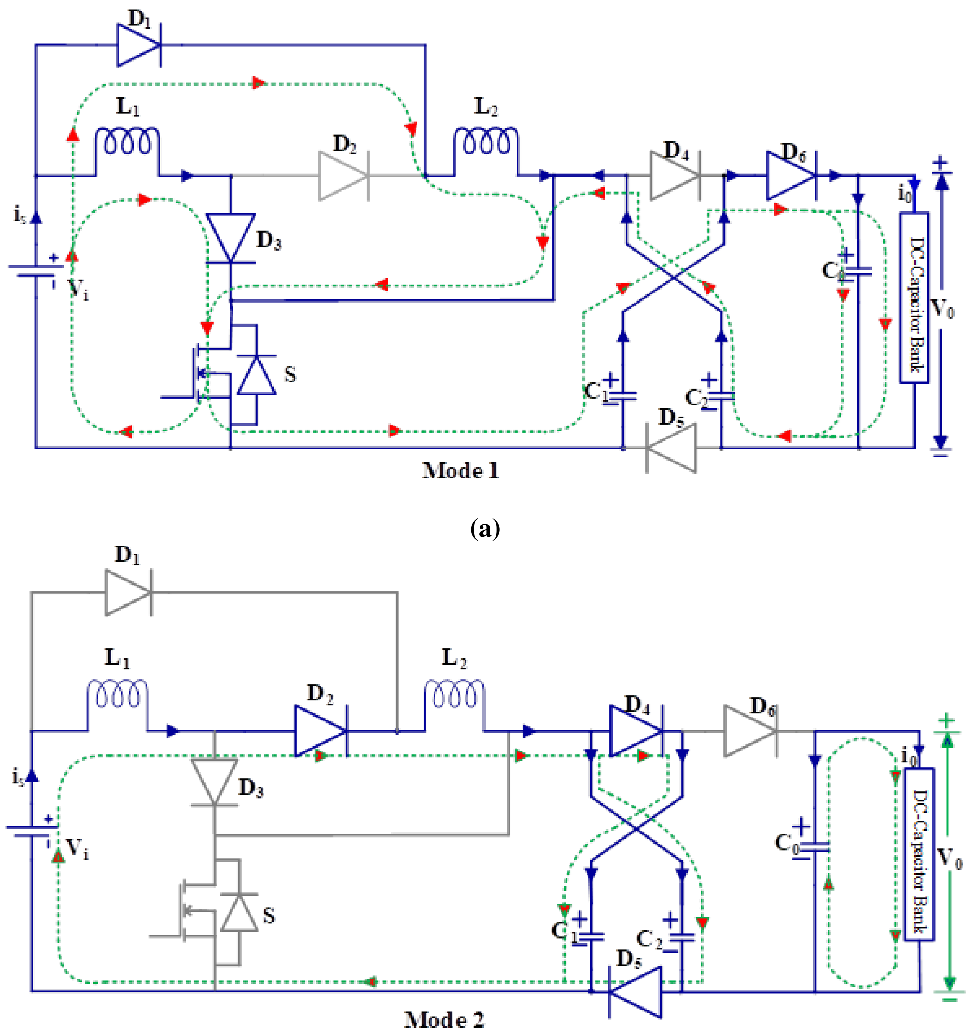

(b)

Figure 2. SSIN converter equivalent circuit. (a) Mode 1. (b) Mode 2.

2.1. CCM operation

2.1.1. Mode 1

This mode activates switch S for $0 \leq t \leq dTS$. The diodes D_1, D_3, D_6 are in forward biased whereas D_2, D_4, D_5 are in reverse biased. Vi parallelly charges the inductors L_1 and L_2. The capacitors C_1 and C_2 discharges power, the output capacitor C_0 charged by supply. Fig. 2(a) displays mode 1's converter equivalent circuit. Inductors L_1 and L_2 voltage is equal to Vi and the output voltage can be $V_0 = V_{C1}$+V_{C2}.

2.1.2. Mode 2

For the duration $dTs \leq t \leq (1-d)TS$, the switch S is off, the diodes D_1, D_3, and D_6 are reverse-biased, whereas D_2,D_4, and D_5 are forward-biased. L_1 and L_2 discharge the energy into series linked capacitors C_1 and C_2. In steady-state, V_{C1}=V_{C2}=$\frac{V_0}{2}$. Fig. 2(b) displays mode 2's converter equivalent circuit. In this mode 2, the L_1, L_2 inductor voltages are given by,

$$V_{L1} = V_{L2} = \frac{2V_i - V_0}{4} \ . \tag{1}$$

Similarly, the output voltage is the same as the voltage across the capacitor V_{C0}, as

$$V_0 = V_{C0} \ . \tag{2}$$

Capacitors linked in series across the point increase the voltage by a factor of 2, in Fig. 1(b), giving the proposed SSIN converter a larger voltage gain than boost converters. CCM analytical waveforms determines the voltage gain. Volt-second balance makes L_1's average voltage zero, which can be given as,

$$V_i d + \frac{2V_i - V_0}{4}(1-d) = 0 \ . \tag{3}$$

In CCM operation, the SSIN converter's DC-voltage gain G_{CCM} is calculated as,

$$G_{CCM} = \frac{V_0}{V_i} = 2\frac{1+d}{1-d} \ . \tag{4}$$

This converter doubles the voltage conversion ratio and produces higher outputs than the many boosting converters. The proposed SSIN converter have only one switch, hence for control pulse, the drive circuits are unnecessary, unless if the closed loop is not required. Equation (5) offers the n-stage SSIN converter's DC-voltage gain, as

$$G_{CCM} = \frac{V_0}{V_i} = 2\frac{1+nd}{1-nd} \ . \tag{5}$$

3. SSIN converter performance and BLDC motor

3.1. SSIN converter design and components

3.1.1. Inductors selection

SSIN converter component design is covered in this section. A 500W SSIN converter components are chosen for 24-volt input, 350-volt output, with 50-kHz switching frequency. The current ripple (δiL) of the inductors L_1 and L_2 during the ON-state of the switch S are computed as,

$$\Delta\, i_{L1} = \frac{V_{in}}{L_1} dTs; \Delta\, i_{L2} = \frac{V_{in}}{L_2} dTs \ . \tag{6}$$

The above current ripple formulas provide the inductance values for L_1 and L_2, as

$$L_1 \geq \frac{V_{in} d}{f_s \Delta\, i_{L1}}; L_2 \geq \frac{V_{in} d}{f_s \Delta\, i_{L2}} \ . \tag{7}$$

Equation (8) shows the average inductor currents $I_L 1$ and $I_L 2$

$$I_{L1} = \frac{2I_0}{(1-d)}; I_{L2} = \frac{2I_0}{(1-d)} \ ; \tag{8}$$

3.1.2. Capacitors selection

While switch S is off, Mode 2 charges C_1 and C_2. C_0 feeds the load. Equations (9a) to (9c) indicate capacitors' charge, as

$$Q_{C1} = C_1 \Delta\, V_{C1} = \frac{I_{L1}}{2} dTs \ , \tag{9a}$$

$$Q_{C2} = C_2 \Delta\, V_{C2} = \frac{I_{L1}}{2} dTs \ , \tag{9b}$$

$$Q_{C0} = C_0 \Delta\, V_0 = I_0(1-d)Ts \ . \tag{9c}$$

I_{in} and I_0 are the average input and output currents. Equation (10) given as

$$V_{in} = 2(\frac{1+d}{1-d})I_0; I_0 = \frac{V_0}{R_0} \ . \tag{10}$$

Equations (9a) to (9c) provide the capacitance values of C_1, C_2, and C_0, as follows,

$$C_1 \geq \frac{dV_0}{(1-d)R_0 f_s \Delta\, V_{C1}} \ , \tag{11}$$

$$C_2 \geq \frac{dV_0}{(1-d)R_0 f_s \Delta\, V_{C2}} \ , \tag{12}$$

$$C_0 \geq \frac{V_0(1-d}{R_0 f_s \Delta\, V_{C0}} \ . \tag{13}$$

3.1.3. Selection of semiconductor devices

Table 1 gives converter component specifications. The switch current and voltage stresses are VS and I_S, and are given by the following equations,

$$\frac{V_S}{V_{in}} = \frac{1+d}{1-d}; I_{S,RMS} = \frac{4\sqrt{d}I_0}{1-d} \ . \tag{14}$$

Below are diode RMS current and voltage stress equations,

$$\frac{V_{D1}}{V_{in}} = \frac{V_{D3}}{V_{in}} = \frac{d}{(1-d)} \ , \tag{15a}$$

$$I_{D1,RMS} = I_{D3,RMS} = \frac{2\sqrt{d}I_0}{(1-d} \ , \tag{15b}$$

$$\frac{V_{D1}}{V_{in}} = 1; I_{D2,RMS} = \frac{2\sqrt{1-d}I_0}{(1-d)} \ , \tag{16}$$

$$\frac{V_{D4}}{V_{in}} = \frac{V_{D5}}{V_{in}} = \frac{V_{D6}}{V_{in}} = \frac{1+d}{1-d} \ , \tag{17}$$

$$I_{D4,RMS} = I_{D5,RMS} = I_{D6,RMS} = \frac{\sqrt{1-d}I_0}{(1-d)} \ . \tag{18}$$

Table 1. SSIN converter component specifications.

Parameter	Specifications
Output Voltage	350V
Input Voltage	24V
Inductors	1.5mH
Switching Frequency	50kHz
Capacitors	100μF

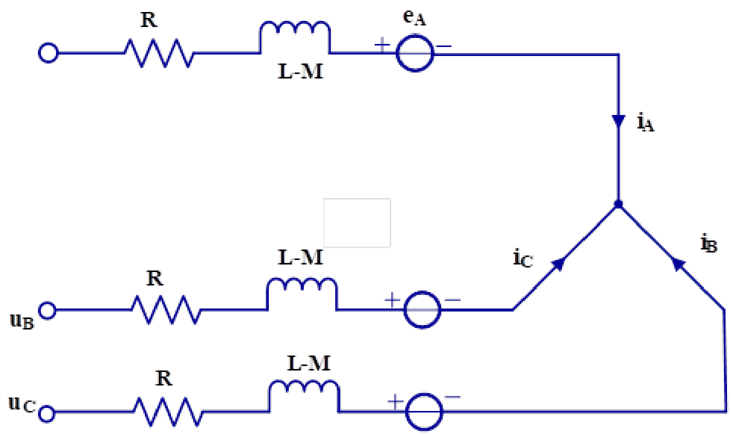

Figure 3. A brushless direct current motor's equivalent circuit.

3.2. Modeling of brushless DC motor

Permanent magnet brushless DC motors are equipped with a trapezoidal back emf. Six power transistors in the three-phase inverter drive two phases of the brushless DC motor, while the third phase is floating. Three stator Hall Effect sensors, electrically linked at 120 degrees, control the inverter's switching. Models for brushless DC motors assume a Y-connected stator with similar resistance in each phase, a faultless switching component in the inverter, and the omission of iron losses such as hysterical losses and core circulating current. Fig. 3 shows an electrical representation of brushless DC motor equivalent circuit.

The magnetic force exerted by a brushless direct current motor can be shown as

$$T_e = \frac{e_A i_A + e_B i_B + e_C i_C}{w_m} \ , \tag{19}$$

where, T_e is electromagnetic torque of a brushless DC motor, ω_m is the angular velocity of rotation measured in radians per second. In order to construct a comprehensive mathematical model of an electromechanical system, the equation that must be used to compute the motion may be shown as

$$T_e - T_L = J\frac{dw_m}{dt} + B_v w_m \ , \tag{20}$$

where, T_L stands for load torque, J for the moment of inertia of the motor, and B_v for the coefficient of viscous friction.

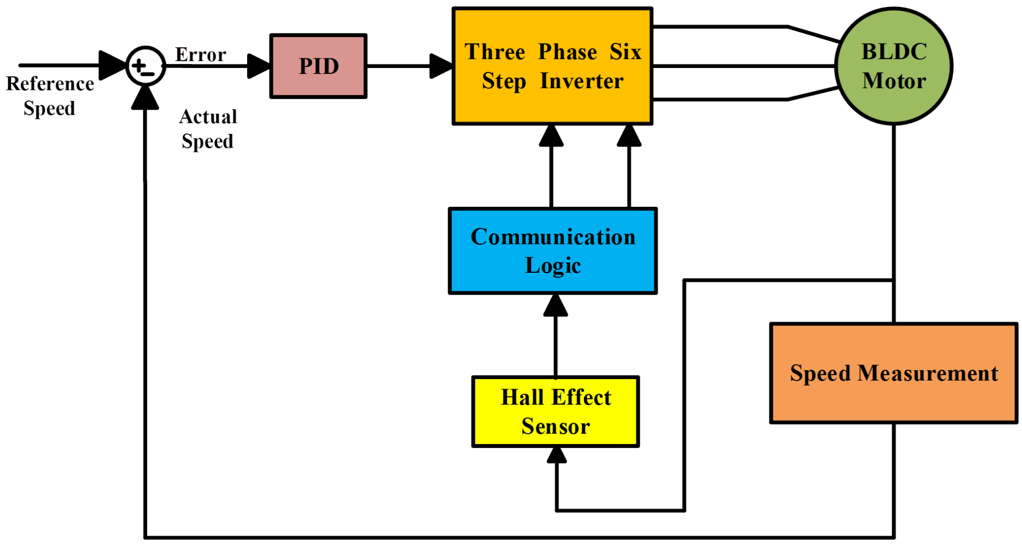

Figure 4. Control of speed in a brushless DC motor using a block diagram.

3.3. Speed control of brushless DC motor

This paper describes PAM-based brushless DC motor speed control. PAM control uses inverter switching commutation to turn power transistors on and off at high rates and drive brushless dc motors. Fig. 4 shows brushless DC motor speed control block diagram. Block diagrams employ two loops. The first loop controls commutation of the inverter with six steps while the second controls brushless DC motor speed.

Hall Effect sensors on brushless DC motors measure position and speed. The algorithm for the Hall Effect sensor switches the inverter, based on rotor position. The rotor spins when the coil is energized. Hall Effect sensors, which measure speed, provide the value of the error.

3.4. Design of PID controller

Even when set point values change, the controller returns the proper answer. Planning includes PID controller design. The block diagram of the PID Controller (Fig. 5) shows P stands for proportional, I is for integral, and D stands for derivative. PID controllers may parallelly integrate excesses on P, I, and D. PID controllers minimize oscillation, rise time, and steady state error. The following equations Equations (21) to (24) are used for the design of PID controller

$$u(s) = [K_p + \frac{K_i}{S} + K_d s]E(S) \ , \tag{21}$$

$$u(t) = K_p e(t) + K_i \int 0^t e(t)dt + K_d \frac{de}{dt} \ , \tag{22}$$

$$T_i = \frac{K_p}{K_i} \ \text{and} \ T_d = \frac{K_d}{K_p} \ , \tag{23}$$

$$u(t) = K_p[e(t) + \frac{1}{T}\int_0^t e(t)dt + T_d \frac{d_e}{dt}] \ , \tag{24}$$

where, K_p denotes proportional gain, K_i denotes integral gain, K_d denotes derivative gain, e denotes error, T_i denotes constant integral time, and T_d denotes constant derivative time.

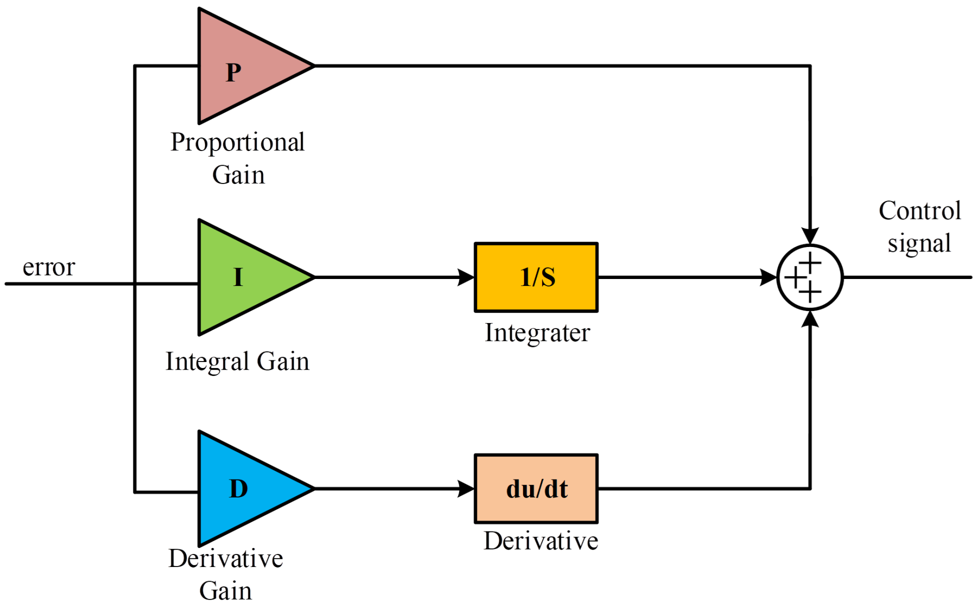

Figure 5. Block diagram of PID controller.

Table 2. The specifications of a BLDC Motor.

Parameters	Value
Stator phase inductance Ls (H)	8.5e-3
Stator phase resistance Rs (ohm)	0.0485
Torque constant (N.m / A_Peak)	0.9552
Back EMF flat area (degrees)	120
Inertia (J(kg.m^2))	0.0027
Viscous damping (F(N.m.s))	0.0004924

4. Simulation results

4.1. SSIN using step up DC-DC converter simulation

Figs. 6(a) and 6(b) show the output voltage V_o and input inductor currents i_{L1} and i_{L2}. The input current is double the inductor current i_{L1}(or i_{L2}) while switch S is ON and equal to it when it is OFF. Fig 7(a)- 7(f) shows the current and voltage of the six diodes D_1, D_2, D_3, D_4, D_5, and D_6. The average currents of inductance L_1 and L_2 are 11.46A and 11.22A, respectively, and their ripple is 3A, which matches the results.

The capacitances C_1, C_2, and C_3 average 165.65V. Fig. 8 represents the Plot of Capacitor Voltage VC1, (b) Plot of Capacitor Voltage VC2. Fig. 10(a) and 10(b) illustrate input and output voltages with lower ripple voltages. Fig 11 shows switching voltage and currents. Simulations show that the suggested converter can deliver substantial voltage gain with little switch voltage stress. Fig. 9(a) and 9(b) illustrate the suggested converter's current curves.

4.2. BLDC motor and its speed control

The simulated parameters of BLDC drive are given in Table 2. Figs. 12(a)–12(f) show the inverter switches gating signals. BLDC motor hall sensor signals are shown in Fig. 13(a)–13(f). In Fig. 14, electromagnetic torque rises and settles after 0.3 seconds. 150V stator back EMF is seen in Fig. 15(a)–15(c). Fig. 16(a), 16(b), and 16(c) show 300V motor input voltages.

A brushless DC motor having a nominal speed of 700 rotations per minute, 48 volts, and 1 kilowatt. simulates. Figs. 17(a) and 18(a) demonstrate PID and traditional PID output response at set points 3000 and 2000 rpm when there was no load. At a fixed point of 3000 rpm and with no load, the PID response has a rising time of 1.1 seconds and -1.751% overshoot. Rise time is 1.15 sec and overshoot is -1.748% at 2000 rpm. The conventional PID The reaction to the set-point of 3000 rpm when there is no load has a rising time of 66 milliseconds and an overshoot of 9.783%.

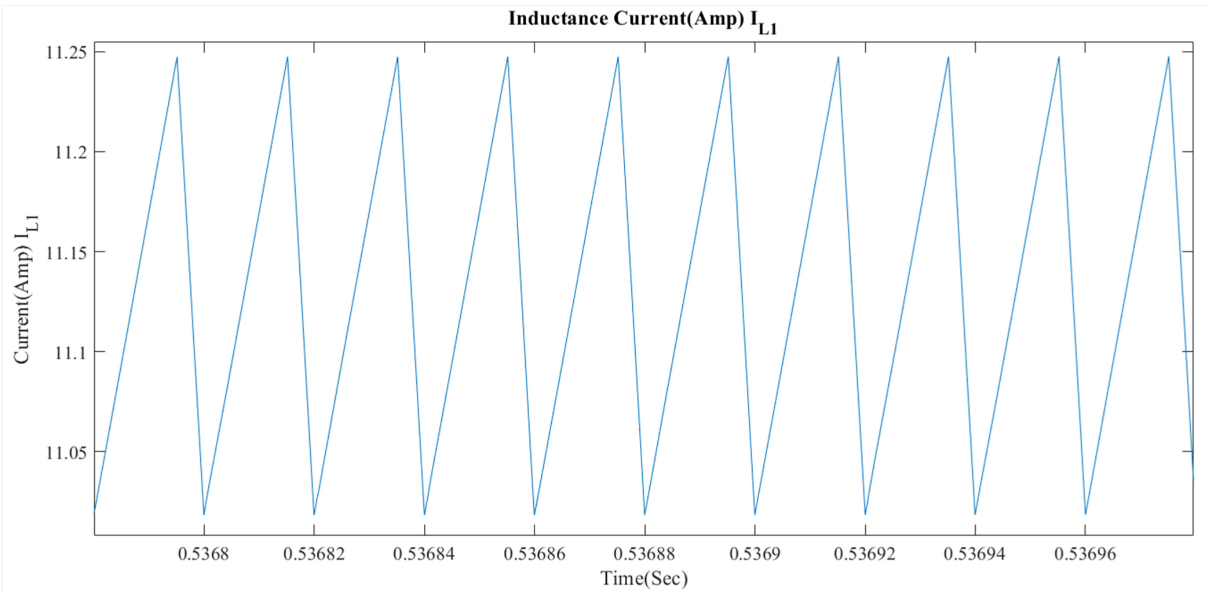

(a)

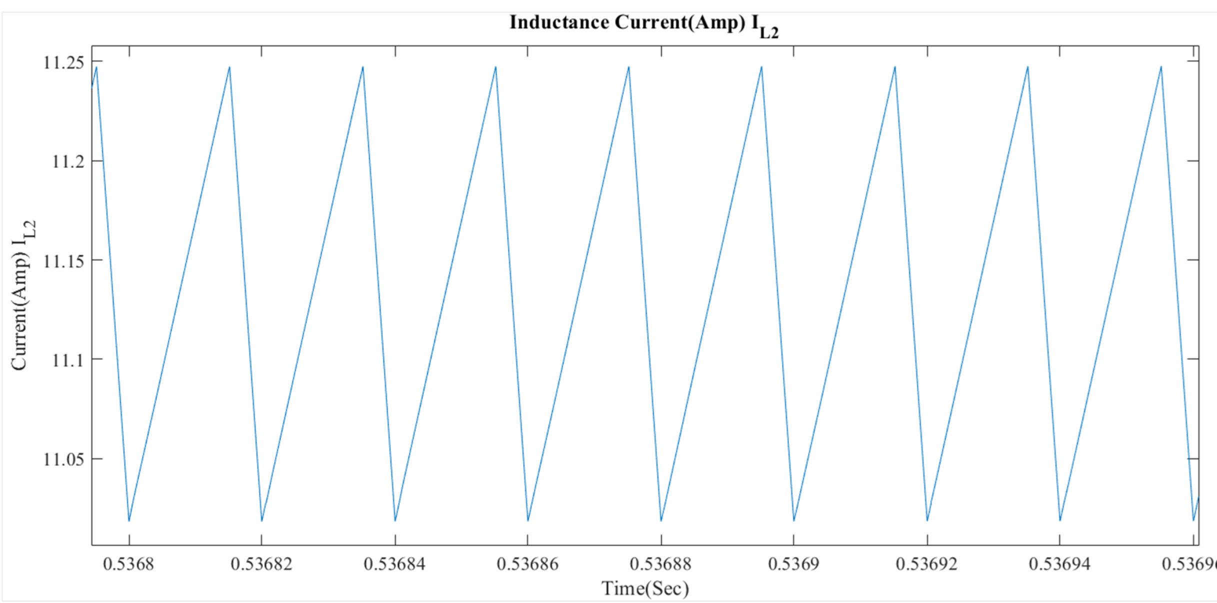

(b)

Figure 6. (a) Plot of current of inductor L1. (b) Plot of current of inductor L2.

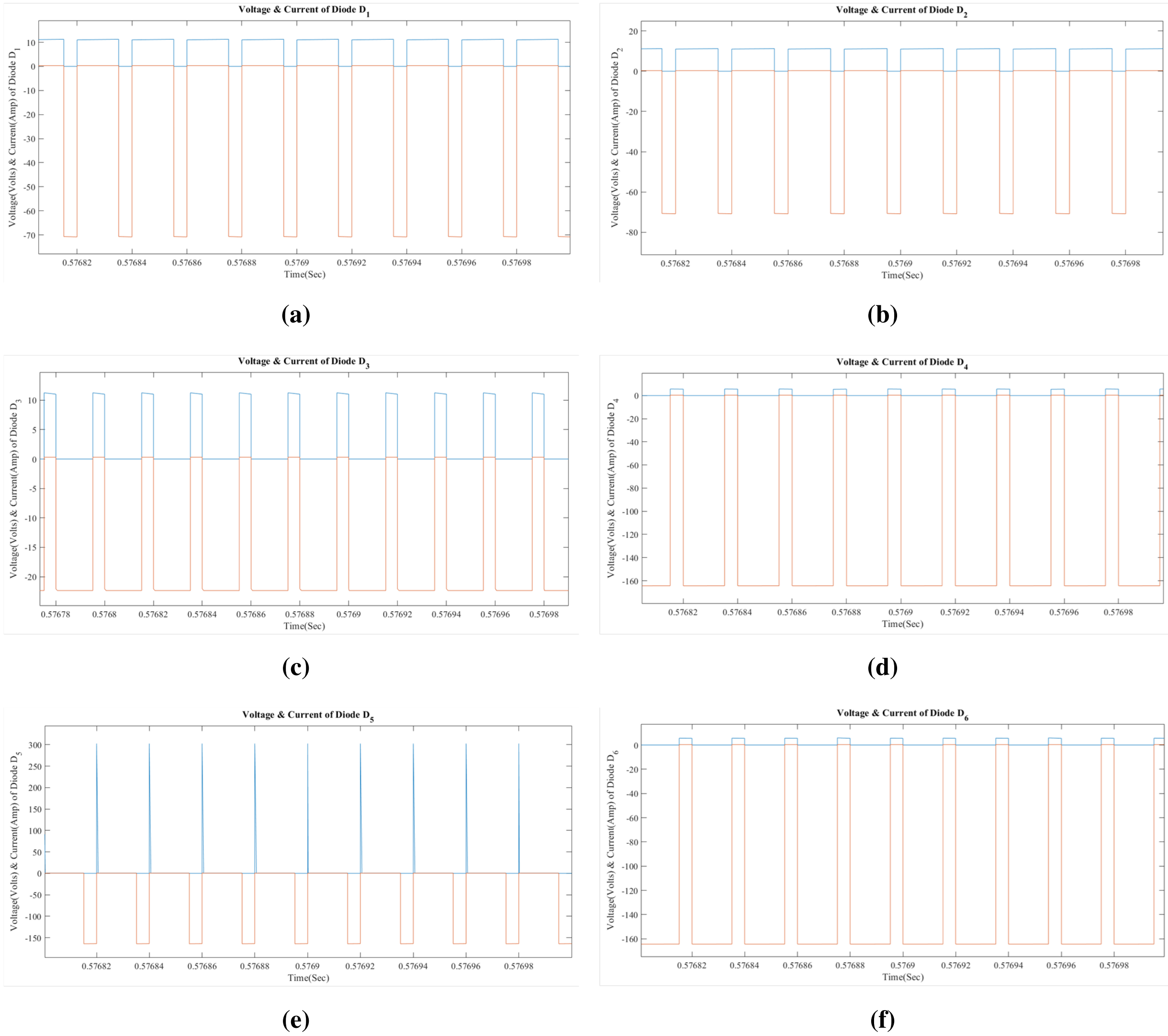

Figure 7. (a)-(f) Plots of voltage and current of diodes D_1-D_6.

At 700 revolutions per minute, the rise time is 68.764 milliseconds, and the overshoot is 7.447%. When there is no load being applied, the speed response reveals an overshoot on the PID, However, it could reach the steady state condition with a settling time of 0.233 seconds when rotating at 3000 revolutions per minute and 0.235 s at 3000 rpm. PID and traditional PID output responses at 3000 and 2000 rpm with 3Nm load are shown in Figs. 17(b) and 18(b).

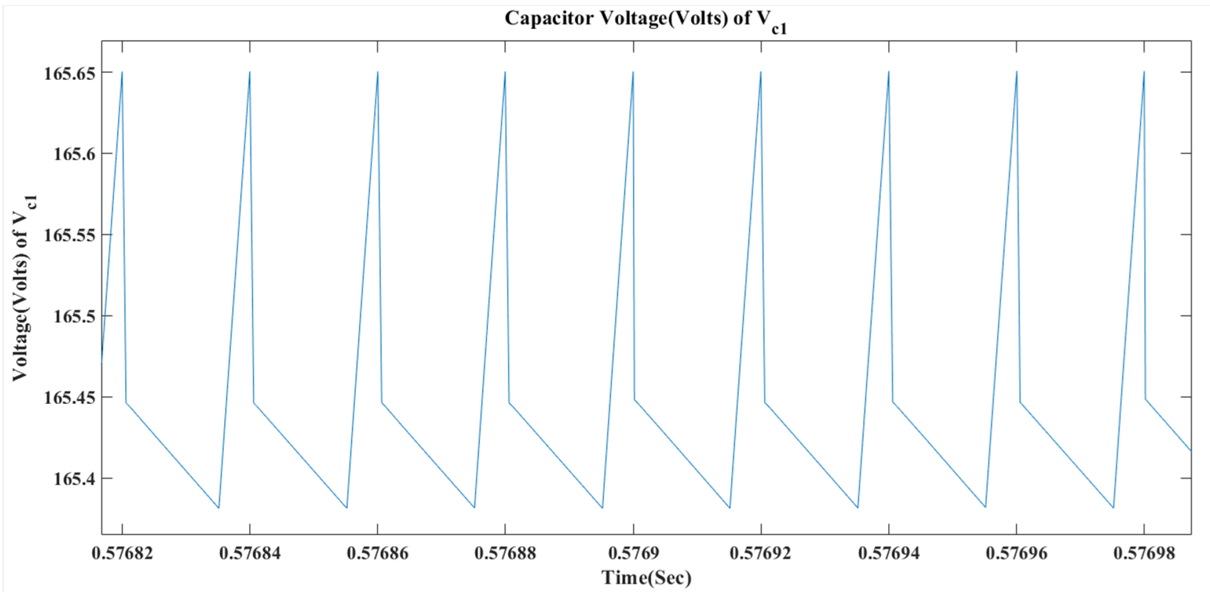

(a)

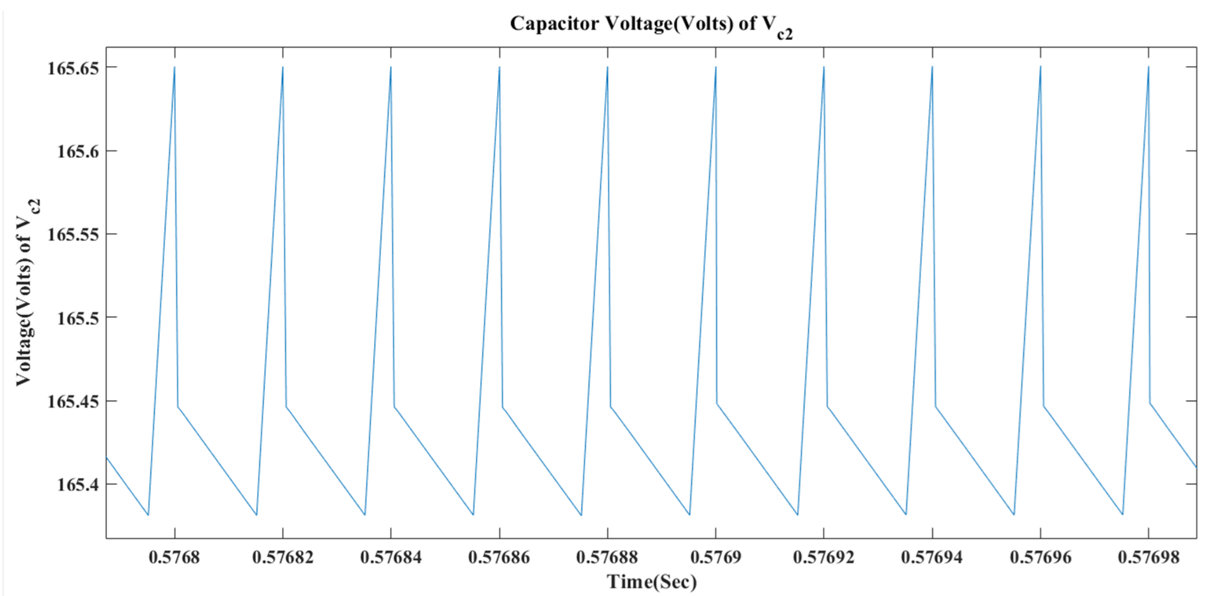

(b)

Figure 8. (a) Plot of capacitor voltage V_{C1}, (b) Plot of capacitor voltage V_{C2}.

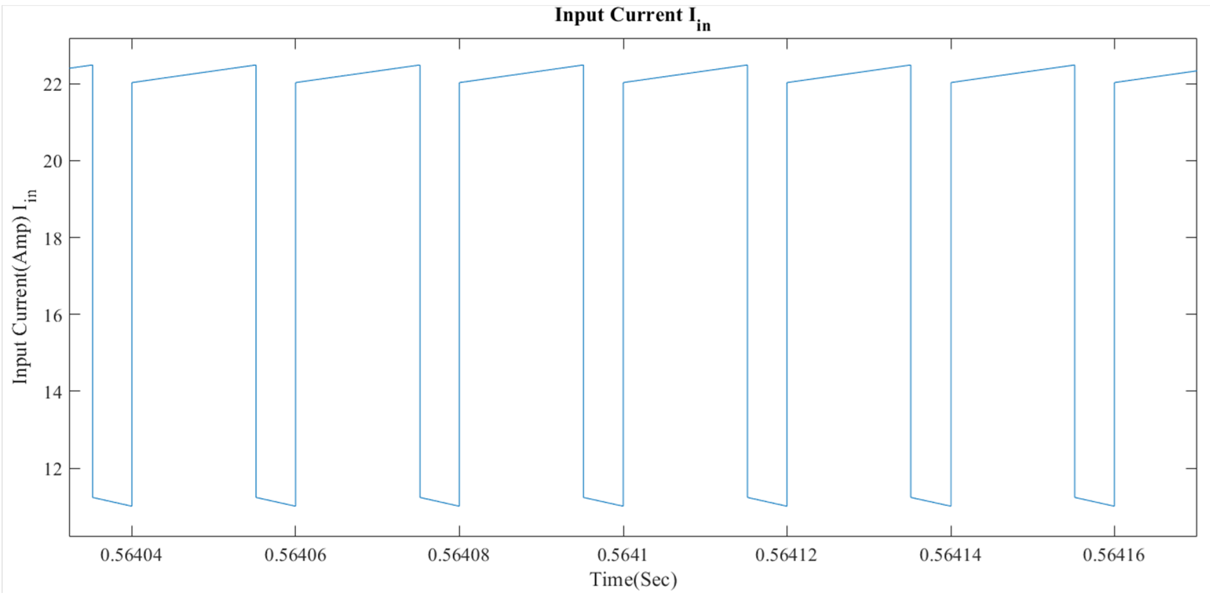

(a)

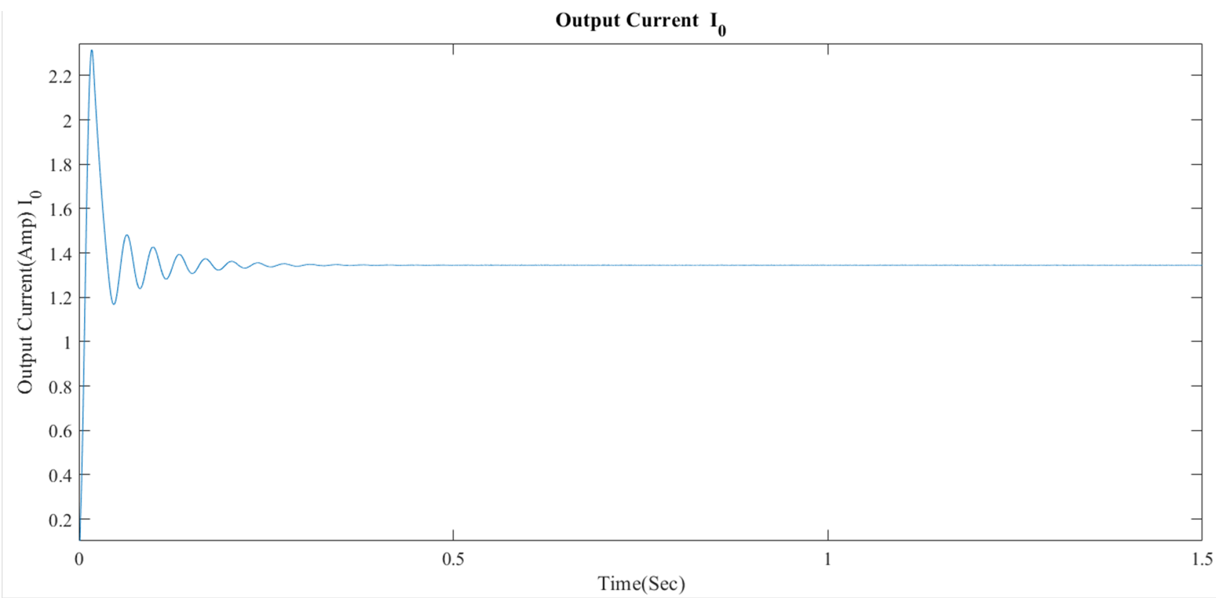

(b)

Figure 9. (a) Plot of input current I_{in}, (b) Plot of output current I_0.

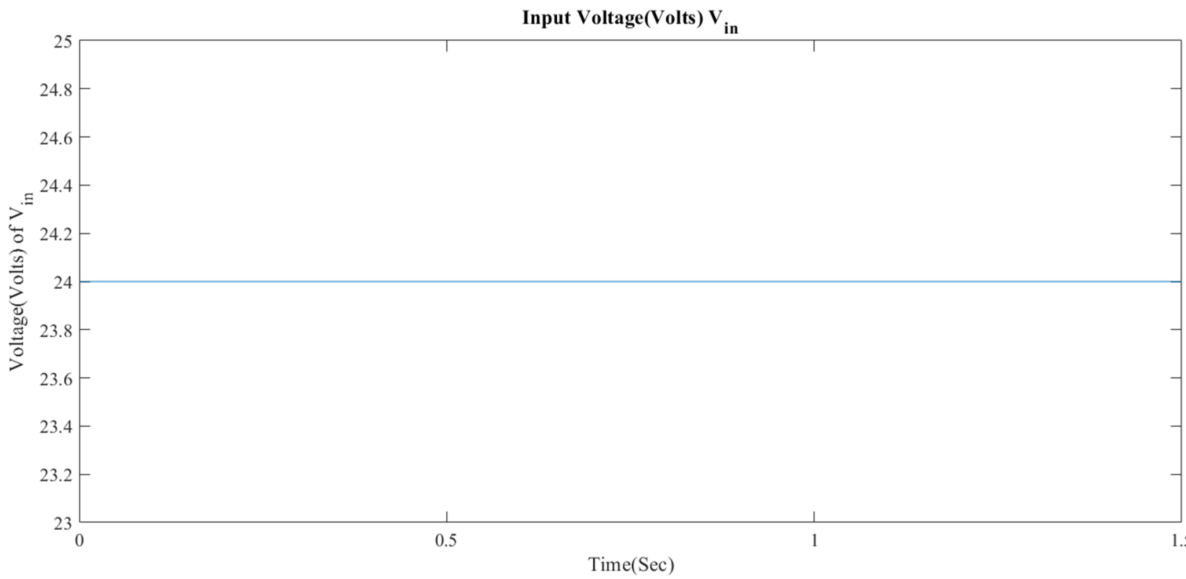

(a)

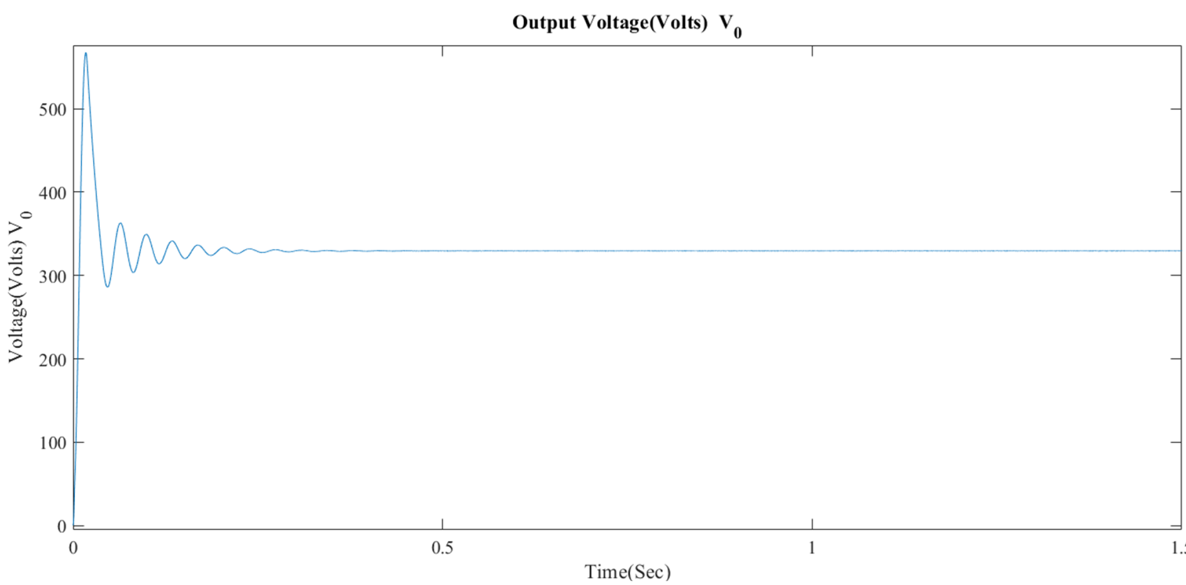

(b)

Figure 10. (a) Plot of input voltage V_{in}, (b) Plot of output voltage V_0.

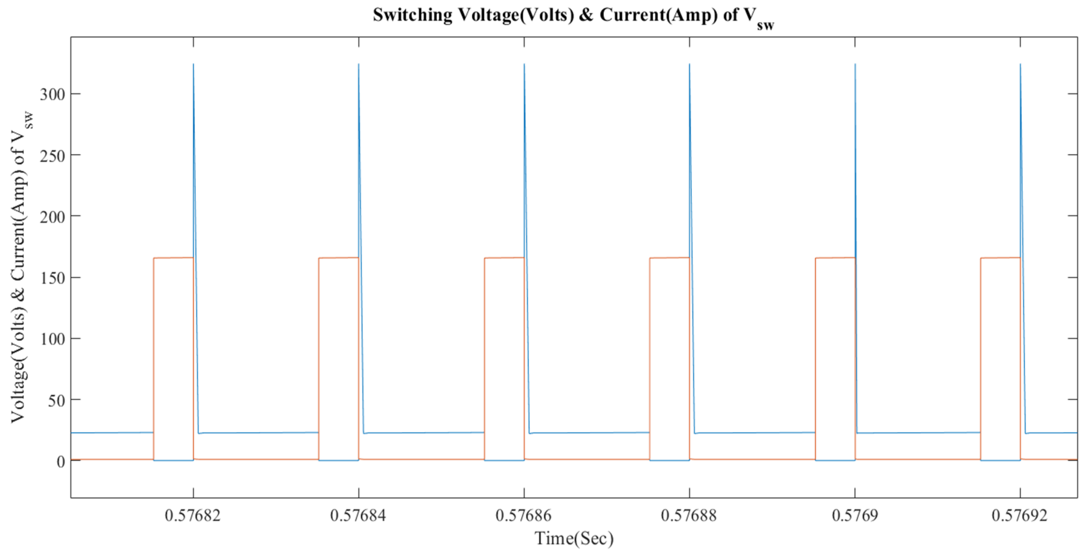

Figure 11. Plot of switching voltage & current of switch V_{sw}

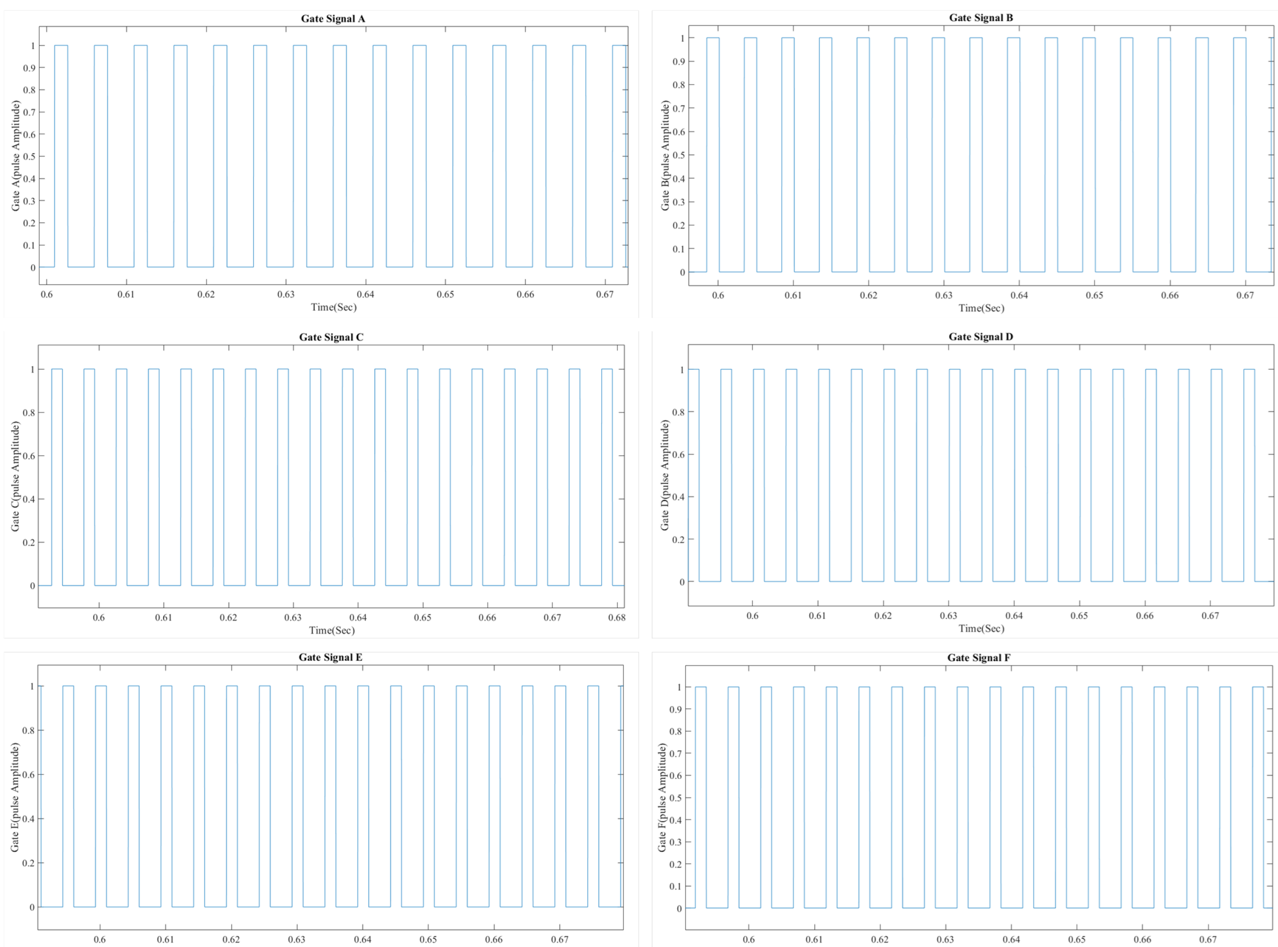

Figure 12. Plots of gate signals from A to F.

Figure 13. Plots of hall sensor signals from A to F.

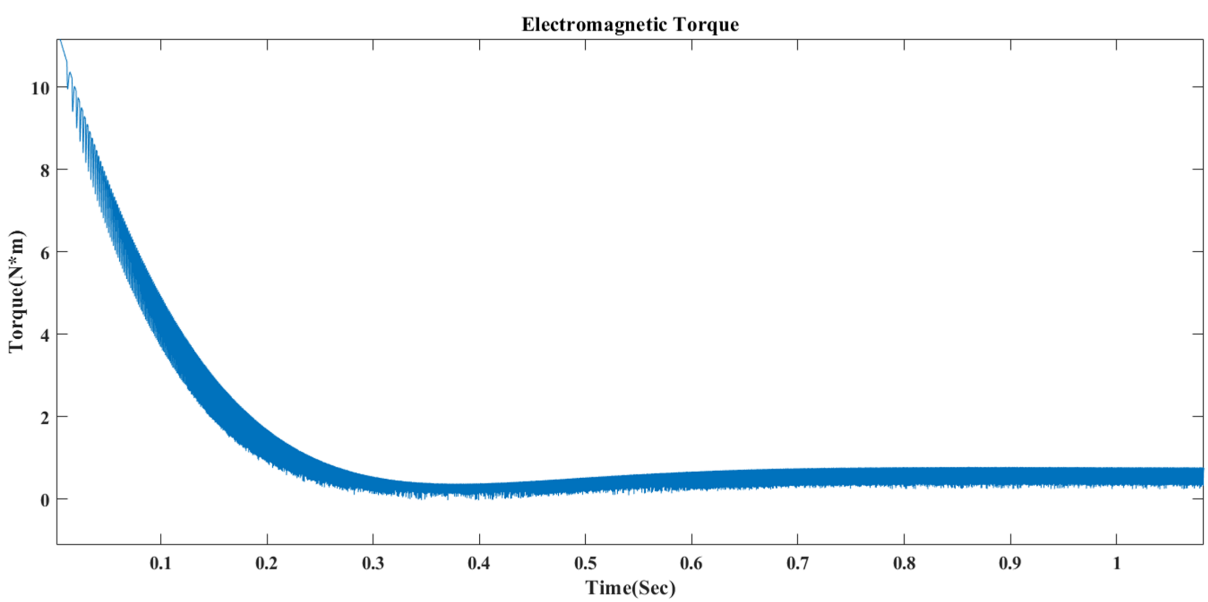

Figure 14. Plot of electromagnetic torque.

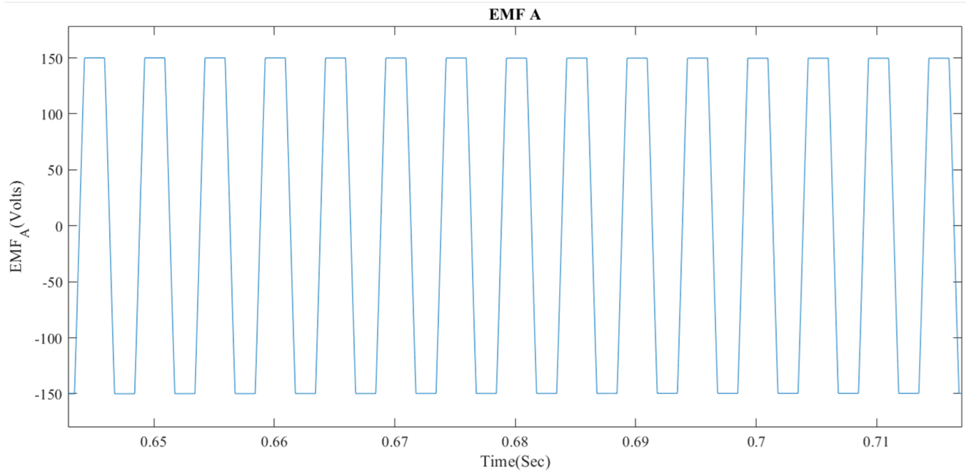

(a)

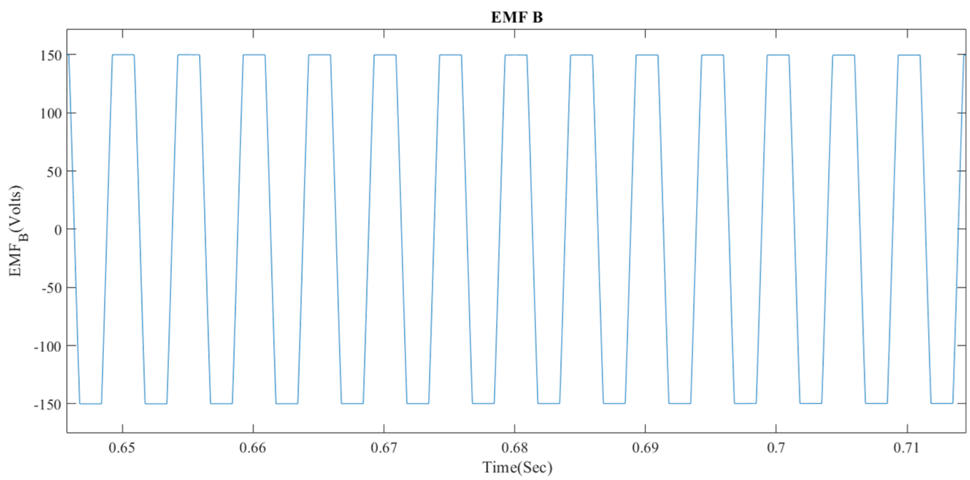

(b)

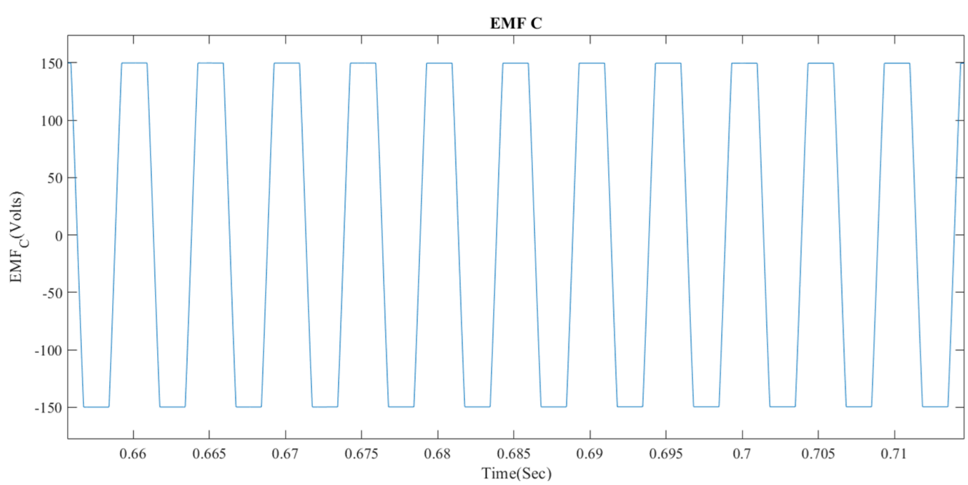

(c)

Figure 15. (a) Plot of stator back EMF of phase A. (b) EMF of phase B. (c) EMF of phase C.

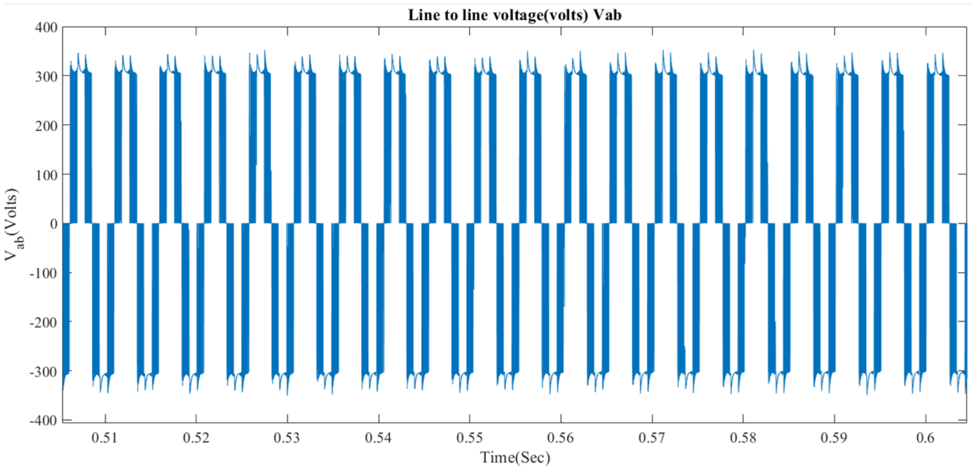

(a)

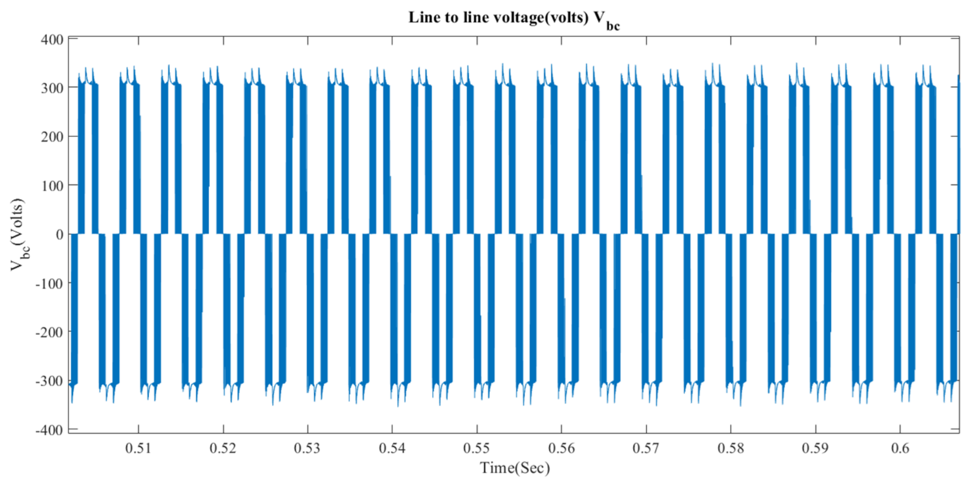

(b)

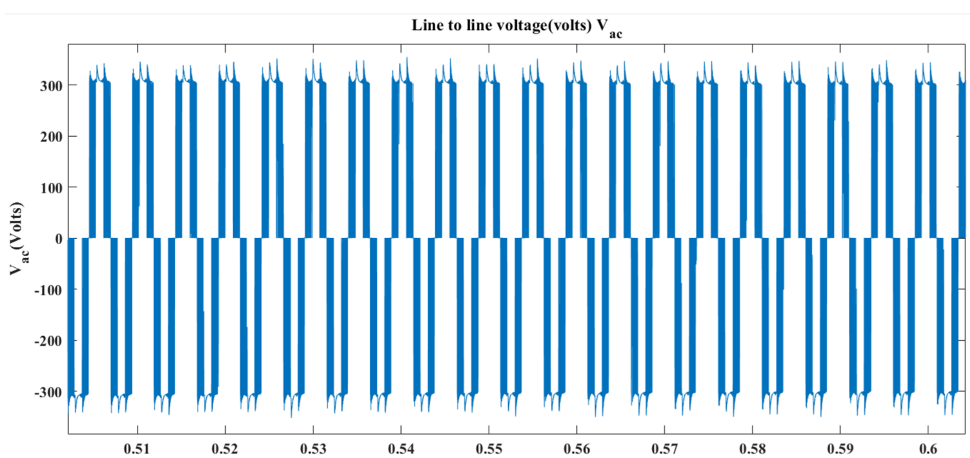

(c)

Figure 16. (a) Plot of Line-to-line Voltage V_{ab}. (b) V_{bc}. (c) V_{ac}.

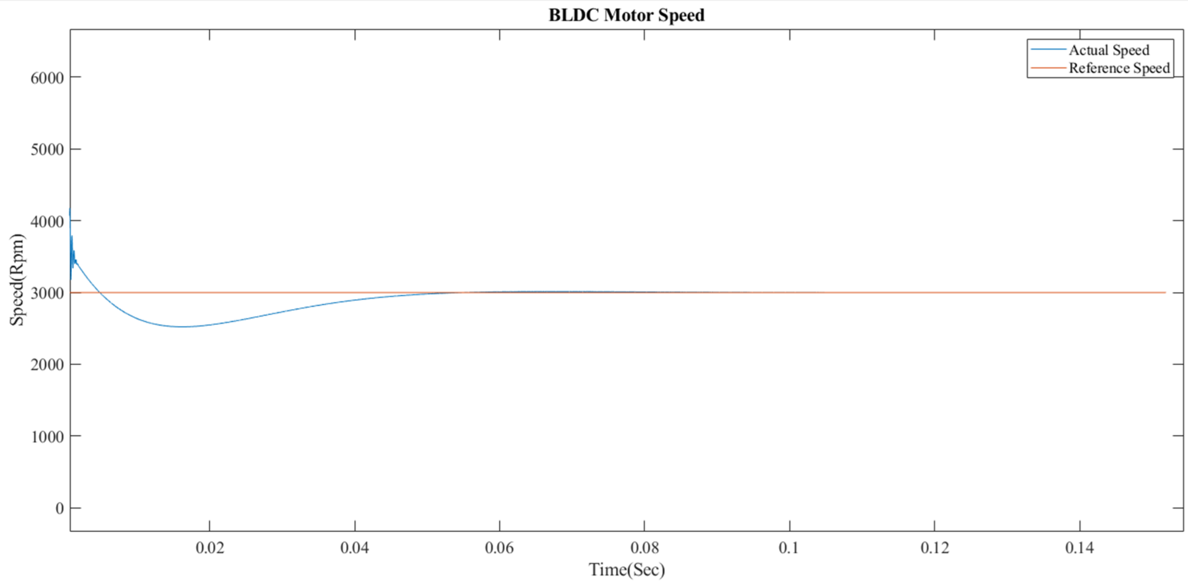

(a)

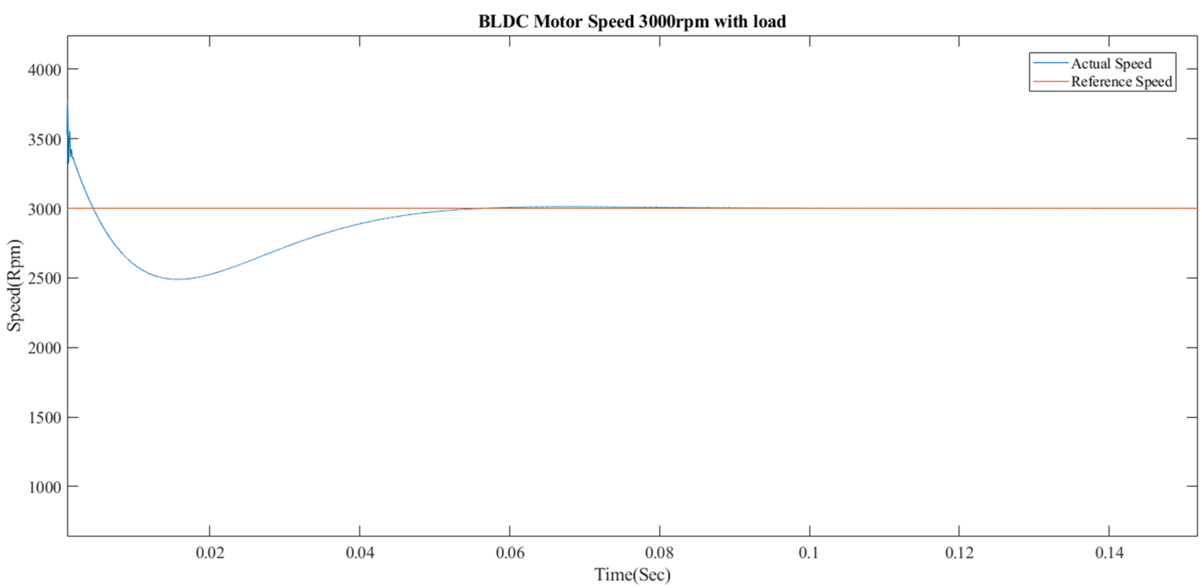

(b)

Figure 17. (a) Plot of Rotor speed at 3000rpm without load. (b) Plot of Rotor speed at 3000rpm with load.

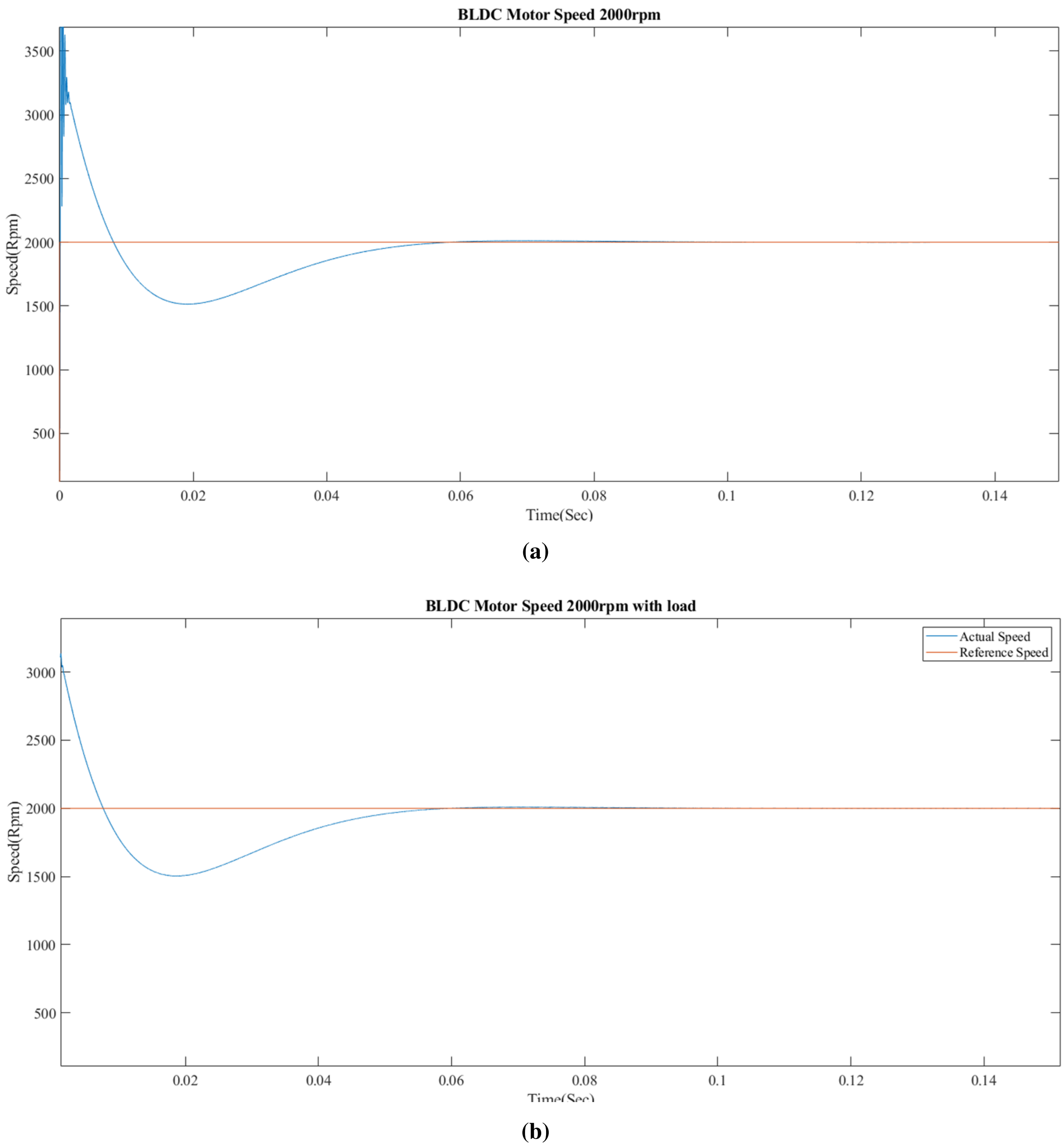

Figure 18. (a) Plot of rotor speed at 2000rpm without load. (b) Plot of Rotor speed at 2000rpm with load.

5. Conclusions

This work introduces an n-stage SSIN converter. The DC-voltage gain of an n-stage SSIN converter may be calculated using analytical waveforms using the formula $2(1 + nd)/(1 - d)$, n-stage converters have $n + 1$ inductors and $3(n + 1)$ diodes. The switching capacitor network in the SSIN boosts voltage output in the region with the lower duty ratio. The SSIN topology's a switch made using a single semiconductor improves converter efficiency regardless of stage count. Deriving the CCM-DCM operational boundary condition. Parasitic components affect voltage gain and efficiency. Thus, the SSIN converter might combine sources of low-voltage direct current such batteries, solar Photo Voltaic, ultra-capacitors, fuel cells etc. Speed-controlled brushless DC motor simulation is shown. The simulation shows that manually tuning PID settings improves the speed of a brushless DC motor under a variety of set point and dynamic load conditions. In electric vehicles with dynamic load conditions and changing set points, a better-tuned PID suggests a faster reaction to steady state.

Funding: This research received no external funding.

Author contributions: Conceptualization: Jeetender Vemula; Methodology: Jeetender Vemula, E. Vidya Sagar; Investigation: Tellapati Anuradha Devi,Gundala Srinivasa Rao; Writing: Jeetender Vemula, and Rekha Rangam; Review and Editing: Jeetender Vemula, E. Vidya Sagar; Supervision: S. Venkata Rami Reddy.

Conceptualization: Jeetender Vemula; Methodology: Jeetender Vemula, E. Vidya Sagar; Investigation: Tellapati Anuradha Devi,Gundala Srinivasa Rao; Writing: Jeetender Vemula, and Rekha Rangam; Review and Editing: Jeetender Vemula, E. Vidya Sagar; Supervision: S. Venkata Rami Reddy.

Disclosure statement: The authors declare no conflict of interest.

References

[1] Wuhua Li and Xiangning He. Review of nonisolated high-step-up dc/dc converters in photovoltaic grid-connected applications. *IEEE Transactions on Industrial Electronics*, 58(4):1239–1250, April 2011.

[2] T. Sreekanth, N. Lakshminarasamma, and Mahesh K. Mishra. A single-stage grid-connected high gain buck–boost inverter with maximum power point tracking. *IEEE Transactions on Energy Conversion*, 32(1):330–339, March 2017.

[3] Sandeep Anand, Saikrishna Kashyap Gundlapalli, and B. G. Fernandes. Transformer-less grid feeding current source inverter for solar photovoltaic system. *IEEE Transactions on Industrial Electronics*, 61(10):5334–5344, October 2014.

[4] Rohit Suryadevara and Leila Parsa. Full-bridge zcs-converter-based high-gain modular dc-dc converter for pv integration with medium-voltage dc grids. *IEEE Transactions on Energy Conversion*, 34(1):302–312, March 2019.

[5] Roger Gules, Walter Meneghette Dos Santos, Flavio Aparecido Dos Reis, Eduardo Felix Ribeiro Romaneli, and Alceu Andre Badin. A modified sepic converter with high static gain for renewable applications. *IEEE Transactions on Power Electronics*, 29(11):5860–5871, November 2014.

[6] Neyyala Raju, N. Murali Mohan, and Vijay Kumar. A switched-inductor switched-capacitor based ultra-gain boost converter: analysis and design. *TESEA, Transactions on Energy Systems and Engineering Applications*, 5(1):1–20, February 2024.

[7] Gang Wu, Xinbo Ruan, and Zhihong Ye. Nonisolated high step-up dc–dc converters adopting switched-capacitor cell. *IEEE Transactions on Industrial Electronics*, 62(1):383–393, January 2015.

[8] L Sri Sivani, L Nagi Reddy, BK SubbaRao, and A Pandian. A new single switch ac/dc converter with extended voltage conversion ratio for smps applications. *Int. Journal of Innovative Technology and Exploring Engineering*, 8(3):68–72, 2019.

[9] Farzad Mohammadzadeh Shahir, Ebrahim Babaei, and Murtaza Farsadi. Voltage-lift technique based nonisolated boost dc–dc converter: Analysis and design. *IEEE Transactions on Power Electronics*, 33(7):5917–5926, July 2018.

[10] Qian Li, Yigeng Huangfu, Liangcai Xu, Jiang Wei, Rui Ma, Dongdong Zhao, and Fei Gao. An improved floating interleaved boost converter with the zero-ripple input current for fuel cell applications. *IEEE Transactions on Energy Conversion*, 34(4):2168–2179, December 2019.

[11] M. Lakshmi and S. Hemamalini. Nonisolated high gain dc–dc converter for dc microgrids. *IEEE Transactions on Industrial Electronics*, 65(2):1205–1212, February 2018.

[12] B. Nagi Reddy, K. Badrinath Shetty, Radhika Jalli, K. Akhila, K. Sai Prudhviraj, and Vadthya Jagan. Reduced redundant power processing in dc-dc converters: A comprehensive review. February 2024.

[13] J.C. Rosas-Caro, J.M. Ramirez, F.Z. Peng, and A. Valderrabano. A dc–dc multilevel boost converter. *IET Power Electronics*, 3(1):129, January 2010.

[14] Mohammad Reza Banaei, Hossein Ardi, and Amir Farakhor. Analysis and implementation of a new single-switch buck–boost dc/dc converter. *IET Power Electronics*, 7(7):1906–1914, July 2014.

[15] Ping Wang, Lei Zhou, Yun Zhang, Jing Li, and Mark Sumner. Input-parallel output-series dc-dc boost converter with a wide input voltage range, for fuel cell vehicles. *IEEE Transactions on Vehicular Technology*, 66(9):7771–7781, September 2017.

[16] Lukas Muller and Jonathan W. Kimball. High gain dc–dc converter based on the cockcroft–walton multiplier. *IEEE Transactions on Power Electronics*, 31(9):6405–6415, September 2016.

[17] Nagi Reddy B, Sahithi Priya Kosika, Manish Patel Gadam, Jagadhishwar Banoth, Ashok Banoth, and Srikanth Koundinya. Analysis of positive output buck-boost topology with extended conversion ratio. *Journal of Energy Systems*, 6(1):62–83, March 2022.

[18] Kerui Li, Yafei Hu, and Adrian Ioinovici. Generation of the large dc gain step-up nonisolated converters in conjunction with renewable energy sources starting from a proposed geometric structure. *IEEE Transactions on Power Electronics*, 32(7):5323–5340, July 2017.

[19] Faqiang Wang. A novel quadratic boost converter with low current and voltage stress on power switch for fuel-cell system applications. *Renewable Energy*, 115:836–845, January 2018.

[20] Neng Zhang, Guidong Zhang, Khay Wai See, and Bo Zhang. A single-switch quadratic buck–boost converter with continuous input port current and continuous output port current. *IEEE Transactions on Power Electronics*, 33(5):4157–4166, May 2018.

[21] Yun Zhang, Heyu Liu, Jing Li, Mark Sumner, and Changliang Xia. Dc–dc boost converter with a wide input range and high voltage gain for fuel cell vehicles. *IEEE Transactions on Power Electronics*, 34(5):4100–4111, May 2019.

[22] Yuanwei Gu, Yanfeng Chen, Bo Zhang, Dongyuan Qiu, and Fan Xie. High step-up dc-dc converter with active switched lc-network for photovoltaic systems. *IEEE Transactions on Energy Conversion*, 34(1):321–329, 2018.

[23] Marcos Antonio Salvador, Telles Brunelli Lazzarin, and Roberto Francisco Coelho. High step-up dc–dc converter with active switched-inductor and passive switched-capacitor networks. *IEEE Transactions on Industrial Electronics*, 65(7):5644–5654, July 2018.

[24] Ebrahim Babaei, Hamed Mashinchi Maheri, Mehran Sabahi, and Seyed Hossein Hosseini. Extendable nonisolated high gain dc–dc converter based on active–passive inductor cells. *IEEE Transactions on Industrial Electronics*, 65(12):9478–9487, December 2018.

[25] B. Nagi Reddy, G. Vinay Kumar, B. Vinay Kumar, B. Jhansi, B. Sandeep, and K. Sarada. Fuel cell based ultra-voltage gain boost converter for electric vehicle applications. *TESEA, Transactions on Energy Systems and Engineering Applications*, 4(1):68–90, June 2023.

[26] Mohammad Maalandish, Seyed Hossein Hosseini, Tohid Jalilzadeh, and Naser Vosoughi. High step-up dc–dc converter using one switch and lower losses for photovoltaic applications. *IET Power Electronics*, 11(13):2081–2092, September 2018.

[27] Farzad Mohammadzadeh Shahir, Ebrahim Babaei, and Murtaza Farsadi. Extended topology for a boost dc–dc converter. *IEEE Transactions on Power Electronics*, 34(3):2375–2384, March 2019.